Islamic University Journal of Applied Sciences (IUJAS)
https://journals.iu.edu.sa/jesc

Volume VII, Issue I, 1 July 2025, Pages 74-96

Exploring VEGFR2 as a Novel Target for Kidney Renal Clear Cell Carcinoma and Molecular Docking-Based Screening of *Garcinia Oblongifolia* Compounds

Abdulwahed Alrehaily[1], Munazzah Tasleem[2,*]

[1] Biology Department, Faculty of Science, Islamic University of Madinah, Madinah 42351, Saudi Arabia, abdulwahed.alrehaily@iu.edu.sa
[2] Department of Public Health, College of Applied Medical Sciences in Al-Namas, University of Bisha, Al-Namas City, Saudi Arabia, munazzah.t@gmail.com, mtaslem@ub.edu.sa

*Corresponding author: Munazzah Tasleem, *Email:* munazzah.t@gmail.com, mtaslem@ub.edu.sa

Abstract

The increasing global cancer burden highlights the urgent need for effective cancer control strategies, particularly for aggressive types like Kidney Renal Clear Cell Carcinoma (KIRC). This study explores the potential of *Garcinia oblongifolia* compounds as targeted inhibitors of Vascular Endothelial Growth Factor Receptor 2 (VEGFR2), a key player in tumor angiogenesis, using *in silico* approach for KIRC using computational approaches to assess their pharmacokinetic properties, toxicity profiles, and binding interactions. The role of VEGFR2 in cancer progression and its correlated genes were identified. A combination of ADMET profiling, bioactivity assessment, and molecular docking was utilized to screen the druglike compounds from *G. oblongifolia.* The study identifies three potential VEGFR2 inhibitors exhibiting a strong pharmacokinetic profile, binding affinity, and moderate bioactivity. The most promising compounds identified from *G. oblongifolia* are PubChem IDs: 11559542, 5280961, and 5281656 as promising VEGFR2 inhibitors with favorable docking energies and interactions with critical residues, including the DFG motif. Docking studies showed that 11559542's Pi-Anion interaction with ASP1046 stabilizes the DFG-out conformation, like Axitinib's hydrogen bonding. Compound PubChem ID:11559542 from *G. oblongifolia*, shows promising electrostatic interactions and moderate bioactivity, therefore, it can be considered a prime candidate for optimization to inhibit VEGFR2. The study supports targeted cancer therapy with natural product derivatives. However, *in vitro* and *in vivo* validation may be required in future studies.

Keywords: VEGFR2, *G. oblongifolia*, Axitinib, Molecular Docking, ADMET, Cancer Therapy, Drug-Likeness, Bioactivity, Targeted Inhibition.

https://doi.org/10.63070/jesc.2025.006
Received 22 April 2024; Revised 19 May 2025; Accepted 24 May 2025.
Available online 25 May 2025.
Published by Islamic University of Madinah on behalf of *Islamic University Journal of Applied Sciences*. This is a free open access article.

1. Introduction

The global cancer burden continues to rise sharply. Current demographic trends suggest that by 2050, the annual incidence of cancer could reach 35 million, marking, which is an estimated 77% increase from the 2022 figures. This alarming increase highlights the urgent need for targeted cancer control initiatives across the globe, as cancer profiles vary widely by region and socioeconomic status. [1] Kidney Renal Clear Cell Carcinoma (KIRC) is the most prevalent and aggressive subtype of renal cell carcinoma (RCC), comprising approximately 70-80% of all RCC cases worldwide. [2-4] KIRC trends in Saudi Arabia are consistent with global trends, indicating a concerning increase in incidence that affects both genders.[5] With the limited availability of effective early detection and treatment methods, it is crucial to explore advanced and targeted therapeutic options for KIRC.

Vascular endothelial growth factor receptors (VEGFRs) are a family of receptor tyrosine kinases that mediate angiogenesis, the formation of new blood vessels needed for normal tissue growth and solid tumor development. VEGFRs consist of an immunoglobulin (Ig)-like extracellular ligand-binding domain, a single transmembrane region, and a signal transduction tyrosine kinase domain. [6] Three major types of VEGFRs: VEGFR1, VEGFR2, and VEGFR3, differ in their ligand specificity and functional roles in vascular and lymphatic biology. Among these VEGFRs, VEGFR2 (kinase insert domain receptor, KDR, or fetal liver kinase-1, FLK-1) is recognized as the primary mediator of angiogenic signaling. [7] This transmembrane glycoprotein, with a molecular weight of 210-230 kDa, is predominantly expressed in vascular and lymphatic endothelial cells, as well as in progenitor and hematopoietic stem cells. [8] VEGFR2 is primarily activated by binding with VEGF-A, a potent pro-angiogenic ligand. Upon ligand binding, VEGFR2 undergoes autophosphorylation at specific tyrosine residues within its intracellular domain, triggering downstream signaling cascades essential for endothelial cell survival, proliferation, and migration. VEGFR2 activates several pathways, some of the key pathways are PI3K/AKT/mTOR, p38 MAPK, and Ras/Raf/MEK/ERK, each of which plays a role in the regulation of cell growth, survival, and angiogenic processes. [9] These pathways drive endothelial cell (EC) mitosis, chemotaxis, and morphogenesis, enabling proliferation, invasion, and new blood vessel formation for physiological and pathological angiogenesis. [10] VEGFR2 is overexpressed in cancers like melanoma, ovarian, thyroid, and other solid tumors. [8, 11] VEGFR2

expression increases cancer cell angiogenic and invasive abilities, which aid tumor growth and metastasis, resulting in poor prognosis. Therefore, VEGF-A/VEGFR2 axis has become a key therapeutic target for anti-angiogenic treatments, with VEGFR2 inhibitors being studied to reduce tumor vascularization and progression. [12] The current treatment strategies to inhibit VEGFR2 rely on tyrosine kinase inhibitors (TKIs). Axitinib, a second-generation TKI, is an indazole derivative with a potency of 50-450 times greater than the first-generation VEGFR inhibitors. These inhibitors selectively inhibit VEGFRs to disrupt angiogenesis, tumor growth, and metastases. [13] However, the use of axitinib is associated with some serious adverse effects [14] requiring the urgency to search for a novel compound with high efficacy and fewer side effects.

The exploration of plant-based therapies offers a promising avenue for cancer treatment, especially due to their potential for fewer side effects and rich phytochemical profiles. Garcinia, in the family Clusiaceae (Guttiferae), is known for its biologically active compounds, particularly polycyclic prenylated acylphloroglucinols and xanthones. [15] These compounds have diverse therapeutic effects, such as anti-inflammatory, antioxidant, antibacterial, antifungal, and cytotoxic, highlighting the genus's pharmaceutical potential. [16] The subtropical regions of southern China and northern Vietnam are the primary habitats of *Garcinia oblongifolia*, a medium-sized shrub. Studies have shown that its bioactive metabolites, oblongifolins and xanthones, are cytotoxic against various cancer cell lines. [15] Several studies have shown that *G. oblongifolia* induces apoptosis and is cytotoxic against cancer cell lines. *G. oblongifolia* contains secondary metabolites like oblongifolin A–G and oblongixanthones A–C, showing apoptotic activity in HeLa cervical cancer cells and cytotoxicity in other cancer models. [17, 18] Li et al. found several phytochemicals in *G. oblongifolia* cytotoxic to MCF-7 breast cancer cells. [19] These findings suggest that *G. oblongifolia* may be a promising VEGFR2 inhibitor for KIRC treatment due to its potent, bioactive compounds that may target cancer cells via apoptosis and cytotoxicity. This study explores VEGFR2 as a primary target for KIRC treatment due to its key role in angiogenesis and cancer progression. Using *in silico* approaches, it aims to identify natural compounds from *G. oblongifolia* with potential efficacy and reduced side effects, offering a promising alternative treatment strategy for KIRC.

2. Materials and Methods

2. 1. Bioinformatics Tools and Databases

In this study, various bioinformatics tools and databases were employed to investigate VEGFR2 expression in KIRC. [20] To analyze VEGFR2 expression levels across various cancers, the Gene Expression Profiling Interactive Analysis (GEPIA2) webserver (http://gepia2.cancer-pku.cn/) was utilized, [21-23]. For the differential gene expression analysis, the ANOVA statistical method was

employed to ensure a robust comparison across the different stages of the disease. To obtain a reliable comparison between tumor and normal tissues, TCGA tumor samples were compared with both TCGA normal and GTEx normal tissues. Additionally, a q-value cutoff of 0.01 was used to control for false positives, providing high confidence in the differential expression results. The UALCAN web portal (http://ualcan.path.uab.edu), [24] was employed to examine VEGFR2 expression across different pathological stages of KIRC. In this study, UALCAN was used to generate VEGFR2 expression box plots, which were categorized based on patients' pathological stages, race, age, tumor metastasis, etc.

2.2. Correlation Between VEGFR2 Expression and Cancer Prognosis

The correlation between VEGFR2 expression and cancer prognosis was evaluated by analyzing overall survival (OS) and disease-free survival (DFS) in patients with Kidney Renal Clear Cell Carcinoma. [20] These analyses were conducted using the GEPIA2 web server to assess the impact of VEGFR2 expression on patient outcomes.

2.3. Correlation Analysis with Other Genes

To explore the relationship between VEGFR2 and other genes with similar expression patterns, a correlation analysis was conducted using the R2 Genomics platform. [25].

2.4. VEGFR2 Protein Network Construction

The functional role of VEGFR2 in cancer was further explored by constructing a protein-protein interaction (PPI) network using the STRING database (https://string-db.org/) [26].

2.5. Pharmacokinetic Analysis of the *G. oblongifolia* Compounds

G. oblongifolia compounds retrieved through PubChem and IMPPAT were selected for ADMET (Absorption, Distribution, Metabolism, Excretion, and Toxicity) analysis using ADMET Lab 2.0 web server (www.admetmesh.scbdd.com). Following the ADMET analysis, compounds that met the drug-likeness criteria were further evaluated for bioactivity against the target protein (VEGFR2) using the CODD-Pred web server [27].

2.6. Target Protein Retrieval

VEGFR2, the target protein three-dimensional x-ray crystal structure was retrieved through the protein data bank (PDB) (https://www.rcsb.org/) with a resolution of 1.95 Å. [2] The target protein, consisting of 316 amino acids, is bound to the anti-cancer drug Axitinib in its binding pocket. [2] The retrieved

protein was cleaned from water molecules and the bound ligands, and corrected for irregular naming, structural disorder, connection between residues, bond ordering, and the absence of side-chain or backbone atoms using iGEMDOCK.[28] iGEMDOCK provides an integrated virtual screening environment that facilitates the entire docking process from preparation through post-screening analysis.

2.7. G. oblongifolia Compound Selection

The compounds derived from *G. oblongifolia*, which passed ADMET properties, were selected for docking studies. These compounds were prepared and optimized for docking into the binding site of VEGFR2 in iGEMDOCK.

2.8. Interaction Analysis and Ranking

Following the molecular docking of the *G. oblongifolia* compounds with VEGFR2, iGEMDOCK generated interaction profiles for each compound with VEGFR2. These interaction profiles were then analyzed to infer pharmacological interactions, which are crucial for understanding the binding mechanisms of the active compounds.

2.9. Visualization of Intra-molecular Interactions of Docked Complexes.

The top-ranked compounds were visualized using Discovery Studio Visualizer v21 and PyMol v2.5 to analyse their binding modes within the VEGFR2 active site.

3. Results

3.1. VEGFR2 Expression in Various Cancer Types

Analysis of data extracted from the TCGA database demonstrated that VEGFR2 expression was significantly elevated across all 27 tumor types (ACC, CESC, COAD, ESCA, GBM, HNSC, KICH: Kidney Chromophobe; KIRC, KIRP, LAML, LGG, LIHC, LUAD, LUSC,MESO: Mesothelioma; OV, PAAD, PCPG, PRAD, READ, SARC, SKCM, STAD, TGCT, THCA, THYM, UCEC, UCS, UVM.), when compared to matched normal tissues from the TCGA and GTEx databases (Figure 1). To further validate these findings, VEGFR2 expression in normal tissues using RNA-sequencing data from the GTEx database was also evaluated. The findings revealed a consistent overexpression of VEGFR2 in all cancer types relative to normal tissues. The differential expression of VEGFR2 between tumor and normal samples was statistically significant across all comparisons, underscoring its potential role in tumorigenesis. Detailed statistical distributions of VEGFR2 expression levels for each tumor type versus normal tissues are presented in Supplementary Data, which illustrates the marked upregulation of VEGFR2 in various cancers.

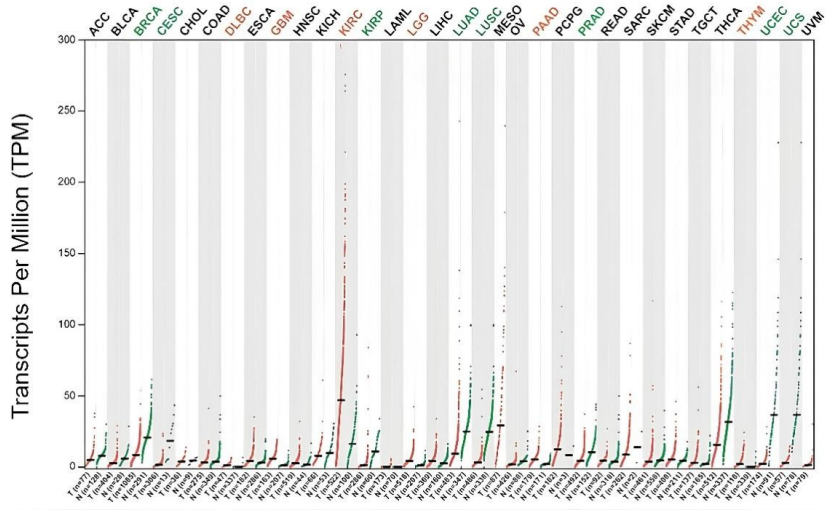

Fig. 1: The chart representing VEGFR2 expression across 27 tumor types using data from TCGA and GTEx, processed through the GEPIA 2.0 web server.

The expression levels of VEGFR2 in KIRC were analyzed across various clinical and demographic variables using the UALCAN web server. The analysis included comparisons based on molecular and histological tumor subtypes, tumor grades, individual cancer stages, patient race, age, gender, and nodal metastasis status. The results revealed statistically significant differences in VEGFR2 expression across various tumor stages when compared to normal tissues. VEGFR2 expression was significantly elevated in primary tumors compared to normal tissues Table 1.

Table 1: VEGFR2 expression in kidney renal clear cell carcinoma using UALCAN.

Comparison Category	Comparison	Statistical Significance (*p*-value)
Individual Cancer Stages	Normal vs. Primary	**1.62×10^{-12}**
	Normal vs. Stage 1	**1.62×10^{-12}**
	Normal vs. Stage 2	**7.70×10^{-5}**
	Normal vs. Stage 3	**2.29×10^{-9}**
	Normal vs. Stage 4	**2.26×10^{-3}**
	Stage 1 vs. Stage 2	**1.82×10^{-2}**
	Stage 1 vs. Stage 3	**2.35×10^{-7}**
	Stage 1 vs. Stage 4	**1.97×10^{-10}**
	Stage 2 vs. Stage 3	0.445 (NS)
	Stage 2 vs. Stage 4	**4.78×10^{-2}**
	Stage 3 vs. Stage 4	0.0622 (NS)
Patient's Race	Normal vs. Caucasian	**$<1 \times 10^{-12}$**
	Normal vs. African American	**6.19×10^{-4}**
	Normal vs. Asian	0.178 (NS)
	Caucasian vs. African American	0.466 (NS)
	Caucasian vs. Asian	0.908 (NS)
	African American vs. Asian	0.859 (NS)
Patient's Gender	Normal vs. Male	**1.62×10^{-12}**
	Normal vs. Female	**1.62×10^{-12}**
	Male vs. Female	**3.56×10^{-3}**
Patient's Age	Normal vs. Age (21-40 Yrs)	**2.62×10^{-3}**

	Normal vs. Age (41-60 Yrs)	**$<1 \times 10^{-12}$**
	Normal vs. Age (61-80 Yrs)	**$<1 \times 10^{-12}$**
	Normal vs. Age (81-100 Yrs)	**1.52×10^{-3}**
	Age (21-40 Yrs) vs. Age (41-60 Yrs)	0.571 (NS)
	Age (21-40 Yrs) vs. Age (61-80 Yrs)	0.823 (NS)
	Age (21-40 Yrs) vs. Age (81-100 Yrs)	0.566 (NS)
	Age (41-60 Yrs) vs. Age (61-80 Yrs)	0.419 (NS)
	Age (41-60 Yrs) vs. Age (81-100 Yrs)	0.0965 (NS)
	Age (61-80 Yrs) vs. Age (81-100 Yrs)	0.231 (NS)
Tumor Grade	Normal vs. Grade 1	**1.52×10^{-3}**
	Normal vs. Grade 2	**1.62×10^{-12}**
	Normal vs. Grade 3	**7.82×10^{-14}**
	Normal vs. Grade 4	**4.89×10^{-2}**
	Grade 1 vs. Grade 2	0.0597 (NS)
	Grade 1 vs. Grade 3	**1.72×10^{-2}**
	Grade 1 vs. Grade 4	**3.60×10^{-3}**
	Grade 2 vs. Grade 3	**1.36×10^{-8}**
	Grade 2 vs. Grade 4	**5.27×10^{-13}**
	Grade 3 vs. Grade 4	**1.56×10^{-3}**
ccRCC Subtype	Normal vs. ccA Subtype	**$<1 \times 10^{-12}$**
	Normal vs. ccB Subtype	**1.48×10^{-6}**
	ccA Subtype vs. ccB Subtype	**4.44×10^{-16}**
Nodal Metastasis	Normal vs. N0	**$<1 \times 10^{-12}$**
	Normal vs. N1	0.474 (NS)
	N0 vs. N1	**4.58×10^{-2}**

3.2. Correlation Between VEGFR2 Expression and Cancer Prognosis

The DFS analysis of the VEGFR2 gene, conducted using GEPIA2, demonstrates a statistically significant difference between high and low VEGFR2 expression groups. The Kaplan-Meier Curve shows two survival curves comparing DFS between patients grouped by VEGFR2 expression levels. The high VEGFR2 group has a 39% reduction in disease recurrence or progression risk compared to the low VEGFR2 group. The hazard ratio is 0.61, indicating a statistically significant difference between the two groups. The log-rank test yielded a *p*-value of 0.0075, further confirming the significant association between VEGFR2 expression and disease-free survival. Both groups included 258 patients, and the follow-up period was extended to 140 months. In addition, the role of VEGFR2 in KIRC progression was evaluated by OS analysis. The OS of VEGFR2, conducted using GEPIA2, reveals a statistically significant difference between patients with high and low VEGFR2 expression. The Kaplan-Meier plot illustrates that patients with high VEGFR2 expression have notably better survival outcomes, with a hazard ratio of 0.49 (p = 9.3e−06), signifying a 51% reduction in the risk of death compared to those with low VEGFR2 expression. The log-rank test yielded a highly significant f-value of 6.1e−06, underscoring the strong association between VEGFR2 expression and overall survival. Both patient groups, high and low VEGFR2, consisted of 258 individuals, and the follow-up duration was extended to 150 months, Figure 2.

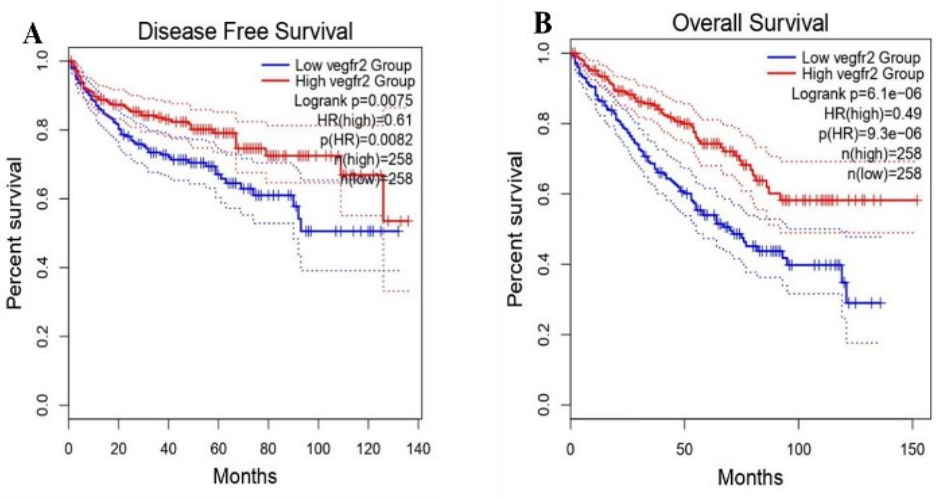

Fig. 2: Kaplan-Meier survival curves for patients grouped by VEGFR2 expression levels. **(A)** Patients with high VEGFR2 expression show improved disease-free survival compared to the low expression group. **(B)** Patients with high VEGFR2 expression exhibit a significantly reduced risk of death

To further validate the role of VEGFR2 in cancer progression, its expression in urinary system cancers such as bladder urothelial carcinoma, kidney chromophobe, renal clear cell, renal papillary cell, and prostate adenocarcinoma was also evaluated. The Kaplan-Meier Curve shows that patients with both high and low VEGFR2 expression have a 10% lower risk of death than those with low expression. However, there is no significant difference in overall survival rates across cancer types. VEGFR2 expression in urinary system cancers does not affect OS. The high VEGFR2 group had a slightly lower mortality risk than the low expression group. VEGFR2 expression in urinary system cancers has no significant effect on DFS. However, the high VEGFR2 group had a slight, non-significant decrease in disease recurrence risk when compared to the low expression group.

3.3. Correlation Analysis with Other Genes

The correlation analysis revealed that a total of 14,044 genes exhibited significant correlations with VEGFR2. Among these, 7,027 genes were found to be positively correlated with VEGFR2. The *p*-values for these positive correlations ranged from 1.72E-216 to 0.0499, indicating highly significant associations. Among the positively correlated genes, several showed extremely high levels of significance. For instance, genes such as VEGFA, KDR, and NRP1, which are known to play critical roles in angiogenesis and vascular development, exhibited strong positive correlations with VEGFR2 (p < 1E-200 for each). These findings suggest a tight regulatory relationship between VEGFR2 and these genes.

3.4. VEGFR2 Protein Network Construction

The top 20 positively correlated genes with VEGFR2 were analyzed using the STRING database with Markov Cluster Algorithm (MCL) clustering to identify functional modules and biological processes. The MCL algorithm identified four distinct clusters based on the protein-protein interaction network. Cluster 1: VEGF Ligand-Receptor Interactions and Tie Signaling Pathway include 11 genes. This cluster is enriched with genes involved in VEGF ligand-receptor interactions and the Tie signaling pathway. Key genes in this cluster include [KDR, FLT1, CDH5, LDB2, TEK, PTPRB, MMRN2, CD34, ERG, and PODXL]. These pathways are crucial for angiogenesis and vascular development, highlighting the central role of VEGFR2 in these processes. [29] The presence of these gene networks suggests that VEGFR2 is tightly linked to the regulation of blood vessel formation and maintenance, which is a critical aspect of tumor growth and metastasis. [8] Cluster 2: Mixed, including Vascular Endothelial Growth Factor Receptor-2 Signaling Pathway and C1q Domain, includes 3 genes. This cluster consists of a mix of genes involved in the VEGFR2 signaling pathway as well as those containing the C1q domain. Genes such as [CYYR1, MYCT1, CLEC14A] may be involved in complement system regulation or other immune-related functions. The presence of these genes suggests a complex interplay between angiogenic and immune responses. This cluster indicates that VEGFR2's role extends beyond angiogenesis, potentially influencing immune modulation within the tumor microenvironment. [30] Cluster 3: IgG-Binding Protein and Presynaptic Active Zone Assembly include 2 genes [PCDH12, PCDH17]. This cluster contains genes associated with IgG-binding proteins and presynaptic active zone assembly. While these functions may seem unrelated to VEGFR2 at first glance, they could indicate novel interactions or regulatory mechanisms that are not immediately apparent. For instance, IgG-binding proteins might be involved in immune evasion strategies employed by cancer cells, while presynaptic active zone assembly genes could suggest unexpected roles for VEGFR2 in neural or synaptic-like interactions within the tumor microenvironment. [31] Cluster 4: includes 2 genes [CALCRL, RAPGEF4] involved in various signaling pathways related to vascular tone regulation and inflammation, while RAPGEF4 plays a role in G-protein signaling [32]. The association of these genes with VEGFR2 suggests additional layers of complexity in vascular signaling and potential cross-talk between different receptor systems that could be exploited therapeutically, Figure 3.

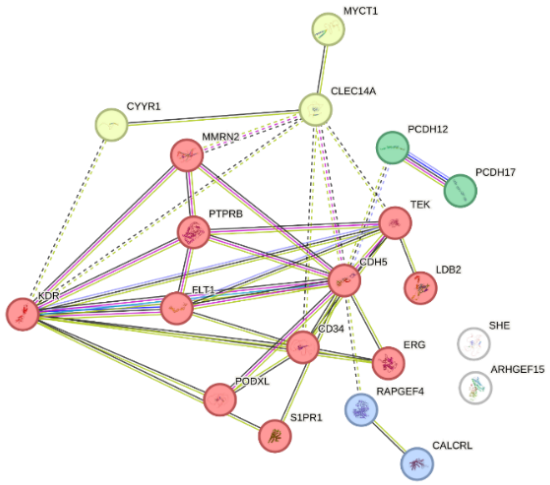

Fig. 3: PPI network for the top 20 genes positively correlated with VEGFR2. The clusters are colored according to their functional enrichment, with node sizes representing the degree of connectivity within the network. Edges: Represent protein-protein interactions based on confidence scores.

3.5. Pharmacokinetic Analysis of the *G. oblongifolia* Compounds

The ADMET analysis of the eleven compounds derived from *G. oblongifolia* was performed utilizing the ADMET Lab 2.0 web server to assess their pharmacokinetic and toxicity parameters. The solubility (LogS) of the compounds was observed to vary. Compound 13037289 exhibited a comparatively high solubility (LogS of -0.712), while compounds 2836049 and 5280961 showed reduced solubility with LogS of -3.4 and -3.5, respectively. The distribution coefficient (LogD) and partition coefficient (LogP) values were predominantly within the acceptable range for most compounds, with values between 2 and 3. Compound 13037289 exhibited a LogD of -1.377 and a LogP of -1.602, indicating increased hydrophilicity. Human intestinal absorption (HIA) predicted values revealed that Compound 13037289 showed the highest HIA value of 0.287, indicating good intestinal absorption. Other compounds exhibited HIA values between 0.008 and 0.169. Caco-2 permeability values demonstrated favorable permeability for the majority of the compounds, with compound 13037289 exhibiting a Caco-2 permeability of -6.258, which is notably favorable. Most of the compounds were predicted with values near zero, thus exhibiting low permeability across the blood-brain barrier (BBB). Compound 13037289 exhibits a higher BBB value of 0.328, indicating moderate BBB permeability. The plasma protein binding (PPB) values for compounds 5280961 and 5281708 were elevated, demonstrating high plasma protein binding at 97.56% and 97.08%, respectively. Conversely, compound 13037289 exhibited a markedly reduced PPB of 16.95%. The volume of distribution at steady state (VDss) exhibited variability, with compounds 11559542 and 14077269 demonstrating moderate to high tissue distribution, with VDss values of approximately 0.879 and 0.908, respectively. Compound 13037289 exhibited a VDss of 0.281, suggesting greater confinement within the plasma. The unbound fraction (Fu) for compound 13037289 was markedly

elevated at 69.04%, indicating reduced plasma protein binding and possibly increased free drug levels in the circulation. Other compounds exhibited Fu values between 1.96% and 17.26%. Clearance (CL) rates exhibited variability, with compound 13037289 demonstrating a CL of 69.04 mL/min/kg, suggesting faster clearance. Other compounds exhibited CL values between 1.57 and 9.473 mL/min/kg. The half-life (T1/2) of the compounds varied from 1.57 to 9.473 hours. Compound 13037289 exhibited a half-life (T1/2) of 1.57 hours, signifying a reduced duration relative to other compounds. The CYP enzyme inhibition profiles of the compounds provide critical insights into their potential for causing drug-drug interactions (DDIs) and affecting the metabolism of co-administered drugs. All the compounds showed moderate inhibition of CYP1A2, CYP2C19, CYP2C9, CYP2D6, and CYP3A4, indicating potential interactions with drugs metabolized by these enzymes, Table 2.

Table 2: Pharmacokinetics parameters of the filtered compound

Compound	LogS	LogD	LogP	HIA (%)	Caco-2	BBB	PPB (%)	VDss	Fu (%)	CL	$T_{1/2}$
2836049	-3.477	2.465	2.523	0.023	-4.738	0.032	92.26	0.672	12.29	7.374	0.823
5280961	-3.44	2.577	2.506	0.01	-4.764	0.02	97.56	0.471	2.09	7.844	0.876
5281631	-3.417	2.591	2.803	0.014	-4.804	0.028	94.89	0.55	8.71	4.408	0.774
5281656	-3.498	1.937	1.878	0.169	-5.082	0.014	91.40	0.658	11.58	9.473	0.908
5281708	-3.464	2.626	2.795	0.008	-4.643	0.054	97.08	0.495	1.96	7.802	0.846
11559542	-3.708	2.084	2.838	0.188	-4.976	0.006	90.40	0.879	14.25	8.338	0.873
13037289	-0.712	-1.377	-1.602	0.287	-6.258	0.328	16.95	0.281	69.04	1.57	0.877
14077269	-3.482	2.537	2.493	0.034	-4.867	0.012	88.22	0.908	16.35	7.64	0.822
25209069	-3.897	2.955	3.795	0.066	-4.946	0.009	95.88	0.693	7.63	3.97	0.674
45269778	-3.944	2.777	3.842	0.06	-4.934	0.01	95.68	0.694	7.73	2.849	0.717
71546261	-3.533	2.536	2.579	0.085	-5.073	0.006	88.47	0.912	17.26	5.979	0.765
Axitinib	-4.849	3.753	3.884	0.021	-4.967	0.628	97.36	0.907	1.45	5.539	0.093

***Abbreviations**: LogS: Aqueous solubility; LogD: Distribution coefficient at physiological pH; LogP: Partition coefficient between octanol and water; HIA: Human intestinal absorption percentage; Caco-2: Permeability across Caco-2 cell lines; BBB: Blood-brain barrier permeability; PPB: Plasma protein binding percentage; Dss: Volume of distribution at steady state; Fu: Fraction unbound in plasma; CL: Clearance rate; T1/2: Half-life of the compound.*

The toxicity profiles of the ADME-filtered compounds were assessed for their potential to cause cardiac arrhythmias, drug-induced liver injury (DILI), Ames mutagenicity, carcinogenicity, skin sensitization, acute aquatic toxicity, and genotoxicity. The compounds showed low hERG inhibition, indicating minimal risk. The compound 2836049 showed moderate DILI risk. The other compounds showed low DILI risk. The Ames mutagenicity tests predicted the compound's potential to cause genetic mutations. The compounds showed moderate Ames mutagenicity. The carcinogenicity tests showed moderate carcinogenicity. The skin sensitization tests showed moderate skin sensitization. The study identifies several compounds with varying carcinogenicity, skin sensitization, and acute aquatic toxicity potentials. Compound 2836049 has a moderate to high carcinogenic potential,

indicating some concern for its effects. Compounds 5280961, 5281631, 5281656, 5281708, 11559542, 13037289, 14077269, 25209069, 45269778, 71546261, and Axitinib all have varying carcinogenic potentials. Skin sensitization is predicted to cause allergic reactions on the skin, with compounds 2836049, 5280961, 5281631, 5281656, 5281708, 11559542, 13037289, 14077269, 25209069, 45269778, 71546261, and Axitinib showing varying levels of sensitization. Acute aquatic toxicity is predicted to cause harm to aquatic organisms. All compounds except 11559542 and 13037289 show no acute aquatic toxicity, while compounds 11559542 and 13037289 show moderate acute aquatic toxicity, indicating some risk. The study concludes that the potential of these compounds to cause cancer, skin sensitization, and acute aquatic toxicity is a significant concern. The study identifies several compounds with varying genotoxicity potentials, each with varying results in genotoxicity assays. Compound 2836049, which has a genotoxic potential of 3, indicates potential genetic damage and is a concern for potential carcinogenic and mutagenic effects. Compound 5280961, which has no genotoxic potential, is unlikely to cause genetic damage. Compound 5281631, which has a genotoxic potential of 3, may cause genetic damage and is a concern for potential carcinogenic and mutagenic effects. Compound 5281708, which has no genotoxic potential, is unlikely to cause genetic damage. Compound 11559542, which has a genotoxic potential of 3, is also a concern for potential carcinogenic and mutagenic effects. Compound 13037289 and Axitinib, have no genotoxic potential and are unlikely to cause genetic damage, as shown in Table 3.

Table 3: Toxicity profiles of the filtered compounds.

Compound	hERG	DILI	Ames	Carcinogenicity	Skin Sensitization	Acute Aquatic Toxicity	Genotoxic
2836049	0.03	0.912	0.684	0.74	0.934	0	3
5280961	0.048	0.51	0.206	0.316	0.926	0	0
5281631	0.019	0.921	0.744	0.819	0.933	0	3
5281656	0.02	0.957	0.538	0.033	0.951	0	3
5281708	0.072	0.52	0.061	0.617	0.895	0	0
11559542	0.002	0.978	0.729	0.083	0.866	2	3
13037289	0.003	0.868	0.036	0.017	0.297	2	0
14077269	0.008	0.96	0.684	0.065	0.682	0	3
25209069	0.008	0.969	0.583	0.689	0.649	0	3
45269778	0.01	0.964	0.546	0.671	0.802	0	3
71546261	0.01	0.968	0.61	0.027	0.716	0	3
Axitinib	0.376	0.978	0.708	0.838	0.087	0	0

Abbreviations: *DILI: Drug-Induced Liver Injury*

The study evaluated the drug-likeness and physical properties of filtered compounds from *G. oblongifolia* using the ADMETLab tool and compared them to Axitinib. The compounds had varying molecular weights, volumetric properties, and compound densities, with most having favorable densities similar to Axitinib's. The analysis revealed a range of molecular weights (MW) from 208.02 to 386.12 g/mol, with most compounds having MWs within the desirable range for drug candidates

(typically < 500 g/mol). However, the number of hydrogen bond acceptors (nHA) and donors (nHD) varied across the compounds, ensuring sufficient binding capabilities. The topological polar surface area (TPSA) values, which are indicative of permeability and bioavailability, ranged from 70.67 to 152.36 Å², with several compounds falling within the optimal range (< 140 Å²), with Axitinib having a TPSA of 70.67 Å². The compounds had a range of rotatable bonds and rings, ensuring stability. The heteroatom counts ranged from 4 to 8, with Axitinib containing 6 heteroatoms. Overall, the compounds met acceptable limits for cell permeability and met the required safety standards.

The predicted pIC50 values provide critical insights into the inhibitory potential of *G. oblongifolia* compounds. The results indicate that the predicted pIC_{50} values for compounds derived from *G. oblongifolia* range from 4.949 to 6.1005, suggesting moderate inhibitory effects on VEGFR2, though less potent than the synthetic drug Axitinib (pIC_{50} = 8.8464). Among these compounds, CID 11559542 exhibits the highest predicted pIC50 of 6.1005, indicating it has the strongest inhibitory potential against VEGFR2 within this group, albeit still weaker than Axitinib. Other compounds, such as CID 5280961 (pIC_{50} = 5.5156) and CID 5281708 (pIC_{50} = 5.4514), also show moderate activity but are less effective than CID 11559542, as shown in Table 4.

Table 4: Drug-likeness and Physical Properties of the filtered compounds

Compound ID	MW	Volume	Density	nHA	nHD	TPSA	nRot	nRing	MaxRing	nHet	pIC_{50}
5281656	260.03	242.021	1.074	6	4	111.13	0	3	14	6	4.949
2836049	228.04	224.441	1.016	4	2	70.67	0	3	14	4	5.3218
71546261	304.06	285.403	1.065	7	3	109.36	2	3	14	7	5.3610
5281631	228.04	224.441	1.016	4	2	70.67	0	3	14	4	5.3686
13037289	208.02	174.745	1.19	8	5	152.36	5	0	0	8	5.3947
14077269	288.06	276.613	1.041	6	2	89.13	2	3	14	6	5.4346
5281708	254.06	256.396	0.991	4	2	70.67	1	3	10	4	5.4514
5280961	270.05	265.186	1.018	5	3	90.9	1	3	10	5	5.5156
45269778	326.08	317.308	1.028	6	3	100.13	0	4	18	6	5.7705
25209069	326.08	317.308	1.028	6	3	100.13	0	4	18	6	5.7738
11559542	360.12	354.587	1.016	7	4	120.36	4	3	14	7	6.1005
Axitinib	386.12	394.491	0.979	5	2	70.67	6	4	9	6	8.8464

Abbreviations: *MW: molecular weight; nHA: number of Hydrogen Acceptor; nHD: number of Hydrogen Donors; TPSA: Topological Polar Surface Area; nRot: number of Rotatable Bonds; nRing: number of Rings; nHet: number of Heteroatoms.*

3.5. Docking and Intramolecular Interaction Analysis

To elucidate the binding modes and affinities of the compounds, a detailed analysis of the intra-molecular interactions and docking energies was conducted. The docking protocol was validated by redocking the bound ligand (Axitinib) to ensure the best pose and conformations of the compounds within the binding pocket Figure 4. Axitinib, the reference compound, exhibited a docking energy of -99.1249 kJ/mol. This value established the standard for evaluating the binding efficacy of the

screened compounds. Compounds 25209069 (-107.037 kJ/mol) and 45269778 (-106.283 kJ/mol) exhibited a greater binding affinity than Axitinib, as indicated by their lower docking energies. This indicates that these compounds may possess greater potential as VEGFR2 inhibitors. Other compounds, including 5281708 (-96.8895 kJ/mol), 5281656 (-96.1814 kJ/mol), and 14077269 (-94.3251 kJ/mol), exhibited binding affinities that were similar yet marginally inferior to that of Axitinib. However, they may still indicate the necessary strength for possible biological activity. The intramolecular interactions between each compound and the active site residues of VEGFR2 elucidate the binding characteristics that influence their docking energies. Hydrogen Bonding are essential for the stabilization of ligand-receptor interactions. Axitinib established critical hydrogen bonds with residues CYS919, ASP1046, and GLU917, indicating that these interactions are vital for high-affinity binding.

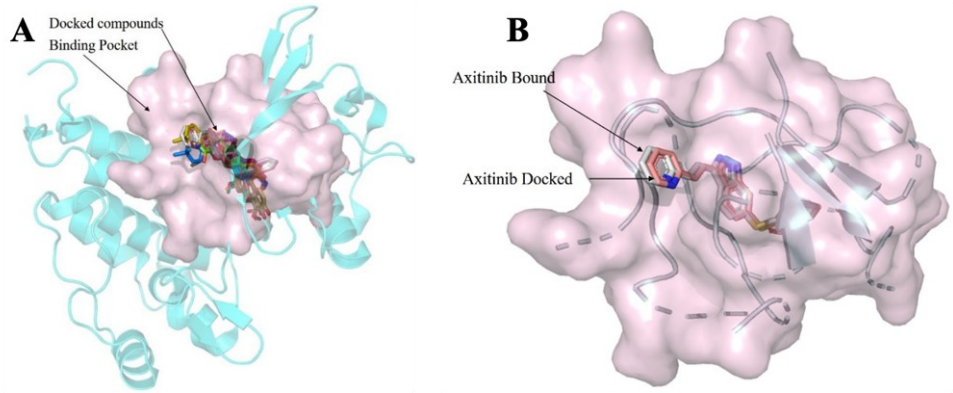

Fig 4: Superimposed docked poses of the compounds within the binding pocket of VEGFR2 (PDB ID: 4AG8_A). (A) all 7 filtered docked compounds, (B) Axitinib re-docked (pink color) and superimposed on top of the bound axitinib (white color). The images were prepared in PyMol software

Compounds such as 25209069, 45269778, and 5280961 formed hydrogen bonds with CYS919, GLU917, and additional residues, thereby strengthening their binding stability within the VEGFR2 pocket. Different forms of Pi-interactions (Pi-Sigma, Pi-Alkyl, Pi-Pi T-shaped) were identified especially with compounds 5280961 and 5281708. The interactions with aromatic residues such as PHE1047 and LEU1035 enhance non-covalent stabilization and affinity in the hydrophobic domains of VEGFR2. Hydrophobic Interactions: Pi-alkyl and Alkyl interactions among hydrophobic residues (e.g., VAL848, LEU840) and the compounds suggest enhanced stabilization. The existence of these interactions, especially with hydrophobic residues along the binding pocket, increases the binding affinity for compounds like 5281631 and 2836049. Additionally, Compound 14077269 formed Conventional H-Bonds with CYS919 and GLU917. Compound 71546261 formed Conventional H-Bonds with VAL899 and GLU885. Compound 11559542 formed Conventional H-Bonds with VAL899, HIS1026, and GLU885. Compound 13037289 formed Conventional H-Bonds with

ASP1046, ILE1044, and ASP1046. It also showed pi-alkyl interactions with VAL848, ALA866, and CYS1045, although it did not exhibit significant pi-sigma or pi-pi interactions, Table 5 and Figure 5.

Table 5: Intramolecular interactions of the filtered compounds with VEGFR2.

Compound	Energy (KJ/mol)	Interacting Residues/atom	Bonds	Distance (Å)
Axitinib	-99.1249	CYS919:N - Axitinib:N14	Conventional H-Bond	3.19075
		ASP1046:N - Axitinib:O81	Conventional H-Bond	3.09339
		Axitinib:N15 - GLU917:O	Conventional H-Bond	2.60243
		Axitinib:N82 - GLU885:OE2	Conventional H-Bond	2.68388
		LYS868:NZ - Axitinib	Pi-Cation	4.30659
		LEU840:CD2 - Axitinib	Pi-Sigma	3.84184
		LYS868:CE - Axitinib	Pi-Sigma	3.87629
		VAL916:CG1 - Axitinib	Pi-Sigma	3.74752
		VAL916:CG2 - Axitinib	Pi-Sigma	3.7007
		LEU1035:CD1 - Axitinib	Pi-Sigma	3.56204
		LEU1035:CD1 - Axitinib	Pi-Sigma	3.44355
		PHE1047 - Axitinib	Pi-Pi T-shaped	5.07704
		Axitinib - VAL848	Pi-Alkyl	4.66309
		Axitinib - ALA866	Pi-Alkyl	4.34327
		Axitinib - VAL899	Pi-Alkyl	5.32773
		Axitinib - CYS1045	Pi-Alkyl	4.54158
		Axitinib - ALA866	Pi-Alkyl	3.47805
		Axitinib - VAL899	Pi-Alkyl	5.4361
		Axitinib - CYS919	Pi-Alkyl	4.63103
		Axitinib - LYS868	Pi-Alkyl	4.44113
		Axitinib - VAL914	Pi-Alkyl	5.41922
25209069	-107.037	CYS919:N - 25209069:O	Conventional H-Bond	2.70523
		25209069:O - LYS920:O	Conventional H-Bond	3.10037
		25209069:O - GLU917:O	Conventional H-Bond	2.598
		LEU1035:CD1 - 25209069	Pi-Sigma	3.98147
		LEU1035:CD1 - 25209069	Pi-Sigma	3.6318
		LEU1035:CD2 - 25209069	Pi-Sigma	3.75093
		PHE1047 - 25209069	Pi-Pi T-shaped	4.94649
		25209069 - LEU840	Pi-Alkyl	4.70298
		25209069 - ALA866	Pi-Alkyl	4.78657
		25209069 - LEU840	Pi-Alkyl	4.2363
		25209069 - LEU1035	Pi-Alkyl	5.2548
		25209069 - VAL848	Pi-Alkyl	4.54718
		25209069 - ALA866	Pi-Alkyl	4.28464
		25209069 - CYS1045	Pi-Alkyl	4.78131
45269778	-106.283	CYS919:N - 45269778:O	Conventional H-Bond	2.81065
		45269778:O - LEU840:O	Conventional H-Bond	2.95195
		45269778:O - GLU917:O	Conventional H-Bond	2.60284
		LEU840:CD1 - 45269778	Pi-Sigma	3.91802
		LEU1035:CD1 - 45269778	Pi-Sigma	3.72339
		LEU1035:CD2 - 45269778	Pi-Sigma	3.9575
		PHE1047 - 45269778	Pi-Pi T-shaped	4.97362
		LEU840 - 45269778	Alkyl	4.58169
		PHE918 - 45269778	Pi-Alkyl	5.24147
		45269778 - LEU840	Pi-Alkyl	4.54399
		45269778 - VAL848	Pi-Alkyl	5.28502
		45269778 - ALA866	Pi-Alkyl	4.62955
		45269778 - VAL848	Pi-Alkyl	4.46262
		45269778 - ALA866	Pi-Alkyl	4.23196

		45269778 - CYS1045	Pi-Alkyl	4.80659
5280961	-103.34	LYS868:NZ - 5280961:O	Conventional H-Bond	2.90977
		CYS919:N - 5280961:O	Conventional H-Bond	2.6787
		5280961:O - GLU917:O	Conventional H-Bond	2.80422
		5280961:O - CYS919:O	Conventional H-Bond	3.10621
		5280961:O - GLU885:OE2	Conventional H-Bond	2.60104
		VAL848:CG1 - 5280961	Pi-Sigma	3.85741
		LEU1035:CD1 - 5280961	Pi-Sigma	3.96931
		CYS1045:SG - 5280961	Pi-Sulfur	4.95121
		PHE1047 - 5280961	Pi-Pi T-shaped	4.76935
		5280961 - LEU840	Pi-Alkyl	5.35438
		5280961 - ALA866	Pi-Alkyl	4.25786
		5280961 - LEU840	Pi-Alkyl	4.59362
		5280961 - ALA866	Pi-Alkyl	4.55077
		5280961 - CYS919	Pi-Alkyl	4.97809
		5280961 - LEU1035	Pi-Alkyl	4.46075
		5280961 - VAL848	Pi-Alkyl	4.87649
		5280961 - LYS868	Pi-Alkyl	5.33532
		5280961 - VAL899	Pi-Alkyl	5.2305
		5280961 - VAL916	Pi-Alkyl	4.9676
5281708	-96.8895	5281708:O - CYS919:O	Conventional H-Bond	2.59244
		5281708:O - GLU885:OE2	Conventional H-Bond	2.74328
		VAL916:CG2 - 5281708	Pi-Sigma	3.7454
		LEU1035:CD1 - 5281708	Pi-Sigma	3.51583
		LEU1035:CD2 - 5281708	Pi-Sigma	3.95338
		CYS1045:SG - 5281708	Pi-Sulfur	5.18604
		PHE1047 - 5281708	Pi-Pi T-shaped	5.79956
		5281708 - VAL848	Pi-Alkyl	5.11677
		5281708 - ALA866	Pi-Alkyl	3.72846
		5281708 - CYS919	Pi-Alkyl	5.36164
		5281708 - LEU840	Pi-Alkyl	4.39773
		5281708 - ALA866	Pi-Alkyl	5.052
		5281708 - CYS919	Pi-Alkyl	5.407
		5281708 - VAL848	Pi-Alkyl	4.91349
		5281708 - ALA866	Pi-Alkyl	5.32516
		5281708 - VAL899	Pi-Alkyl	4.87163
5281656	-96.1814	CYS919:N - 5281656:O	Conventional H-Bond	2.73867
		5281656:O - GLU917:O	Conventional H-Bond	2.68195
		5281656:O - ASP1046:O	Conventional H-Bond	2.91039
		5281656:O - ASP1046:O	Conventional H-Bond	2.83777
		5281656:O - CYS919:O	Conventional H-Bond	3.39695
		GLY922:CA - 5281656:O	Carbon Hydrogen Bond	3.71414
		VAL848:CG2 - 5281656	Pi-Sigma	3.7265
		LEU1035:CD1 - 5281656	Pi-Sigma	3.7277
		LEU1035:CD1 - 5281656	Pi-Sigma	3.88607
		LEU1035:CD2 - 5281656	Pi-Sigma	3.97769
		CYS1045:SG - 5281656	Pi-Sulfur	4.41821
		PHE1047 - 5281656	Pi-Pi T-shaped	4.83428
		PHE1047 - 5281656	Pi-Pi T-shaped	4.52794
		5281656 - VAL848	Pi-Alkyl	4.46375
		5281656 - ALA866	Pi-Alkyl	4.28507
		5281656 - CYS1045	Pi-Alkyl	4.97832
		5281656 - LEU840	Pi-Alkyl	4.82572
		5281656 - ALA866	Pi-Alkyl	4.43956
		5281656 - CYS919	Pi-Alkyl	4.94823
14077269	-94.3251	CYS919:N - 14077269:O	Conventional H-Bond	2.84942
		14077269:O - GLU917:O	Conventional H-Bond	2.59544
		LEU840:CD1 - 14077269	Pi-Sigma	3.98039

		LEU1035:CD1 - 14077269	Pi-Sigma	3.97496
		LEU1035:CD1 - 14077269	Pi-Sigma	3.31407
		LEU1035:CD2 - 14077269	Pi-Sigma	3.74952
		PHE1047 - 14077269	Pi-Pi T-shaped	4.90429
		14077269:C - LEU840	Alkyl	4.13017
		PHE1047 - 14077269:C	Pi-Alkyl	4.66585
		14077269 - LEU840	Pi-Alkyl	4.70855
		14077269 - ALA866	Pi-Alkyl	4.78206
		14077269 - LEU1035	Pi-Alkyl	5.48777
		14077269 - VAL848	Pi-Alkyl	4.85079
		14077269 - ALA866	Pi-Alkyl	4.52871
		14077269 - VAL899	Pi-Alkyl	5.49893
		14077269 - CYS1045	Pi-Alkyl	4.50775
71546261	-91.1924	VAL899:N - 71546261:O	Conventional H-Bond	3.22905
		71546261:O - GLU885:OE2	Conventional H-Bond	3.04376
		71546261:O - VAL899:O	Conventional H-Bond	3.15284
		ILE1044:CG2 - 71546261	Pi-Sigma	3.75842
		71546261:C - ILE1044	Alkyl	4.1177
		HIS1026 - 71546261:C	Pi-Alkyl	5.10816
		71546261 - VAL898	Pi-Alkyl	4.85873
11559542	-90.4886	VAL899:N - 11559542:O	Conventional H-Bond	3.14158
		HIS1026:N - 11559542:O	Conventional H-Bond	3.10976
		11559542:O - VAL899:O	Conventional H-Bond	3.38128
		11559542:O - ILE1044:O	Conventional H-Bond	2.60218
		11559542:O - GLU885:OE1	Conventional H-Bond	3.07746
		CYS1045:CA - 11559542:O	Carbon Hydrogen Bond	3.52225
		ASP1046:OD2 - 11559542	Pi-Anion	4.62774
		HIS1026 - 11559542	Pi-Pi Stacked	5.334
		HIS1026 - 11559542	Pi-Pi Stacked	5.36876
		11559542:C - VAL898	Alkyl	5.31803
		11559542:C - ILE1044	Alkyl	3.69172
		HIS1026 - 11559542:C	Pi-Alkyl	5.32881
		11559542 - LEU889	Pi-Alkyl	5.4023
		11559542 - ILE892	Pi-Alkyl	5.4628
		11559542 - VAL898	Pi-Alkyl	5.0011
		11559542 - ILE1044	Pi-Alkyl	5.16762
5281631	-88.6991	CYS919:N - 5281631:O	Conventional H-Bond	2.69628
		5281631:O - GLU917:O	Conventional H-Bond	2.67126
		5281631:O - LYS920:O	Conventional H-Bond	3.16611
		LEU840:CD1 - 5281631	Pi-Sigma	3.95807
		VAL848:CG1 - 5281631	Pi-Sigma	3.7799
		LEU1035:CD1 - 5281631	Pi-Sigma	3.96353
		PHE1047 - 5281631	Pi-Pi T-shaped	5.00615
		5281631 - VAL848	Pi-Alkyl	5.35862
		5281631 - ALA866	Pi-Alkyl	4.71368
		5281631 - LEU1035	Pi-Alkyl	4.56027
		5281631 - ALA866	Pi-Alkyl	4.02683
		5281631 - LEU840	Pi-Alkyl	3.9995
2836049	-84.4535	CYS919:N - 2836049:O	Conventional H-Bond	3.07959
		2836049:O - CYS919:O	Conventional H-Bond	2.60013
		2836049:O - ASP1046:O	Conventional H-Bond	3.10218
		2836049:O - PHE918	Pi-Donor Hydrogen Bond	3.86574
		LEU840:CD1 - 2836049	Pi-Sigma	3.98177
		VAL848:CG1 - 2836049	Pi-Sigma	3.81828
		VAL848:CG2 - 2836049	Pi-Sigma	3.78932
		LEU1035:CD1 - 2836049	Pi-Sigma	3.99694
		CYS1045:SG - 2836049	Pi-Sulfur	4.45796
		PHE1047 - 2836049	Pi-Pi T-shaped	4.61496

		PHE1047 - 2836049	Pi-Pi T-shaped	4.78059
		2836049 - ALA866	Pi-Alkyl	4.39692
		2836049 - CYS1045	Pi-Alkyl	4.91694
		2836049 - VAL848	Pi-Alkyl	5.33154
		2836049 - ALA866	Pi-Alkyl	4.45672
		2836049 - LEU1035	Pi-Alkyl	4.50828
13037289	-70.7654	ASP1046:N - 13037289:O	Conventional H-Bond	3.13407
		13037289:H - ILE1044:O	Conventional H-Bond	2.75883
		13037289:H - ASP1046:O	Conventional H-Bond	1.99263

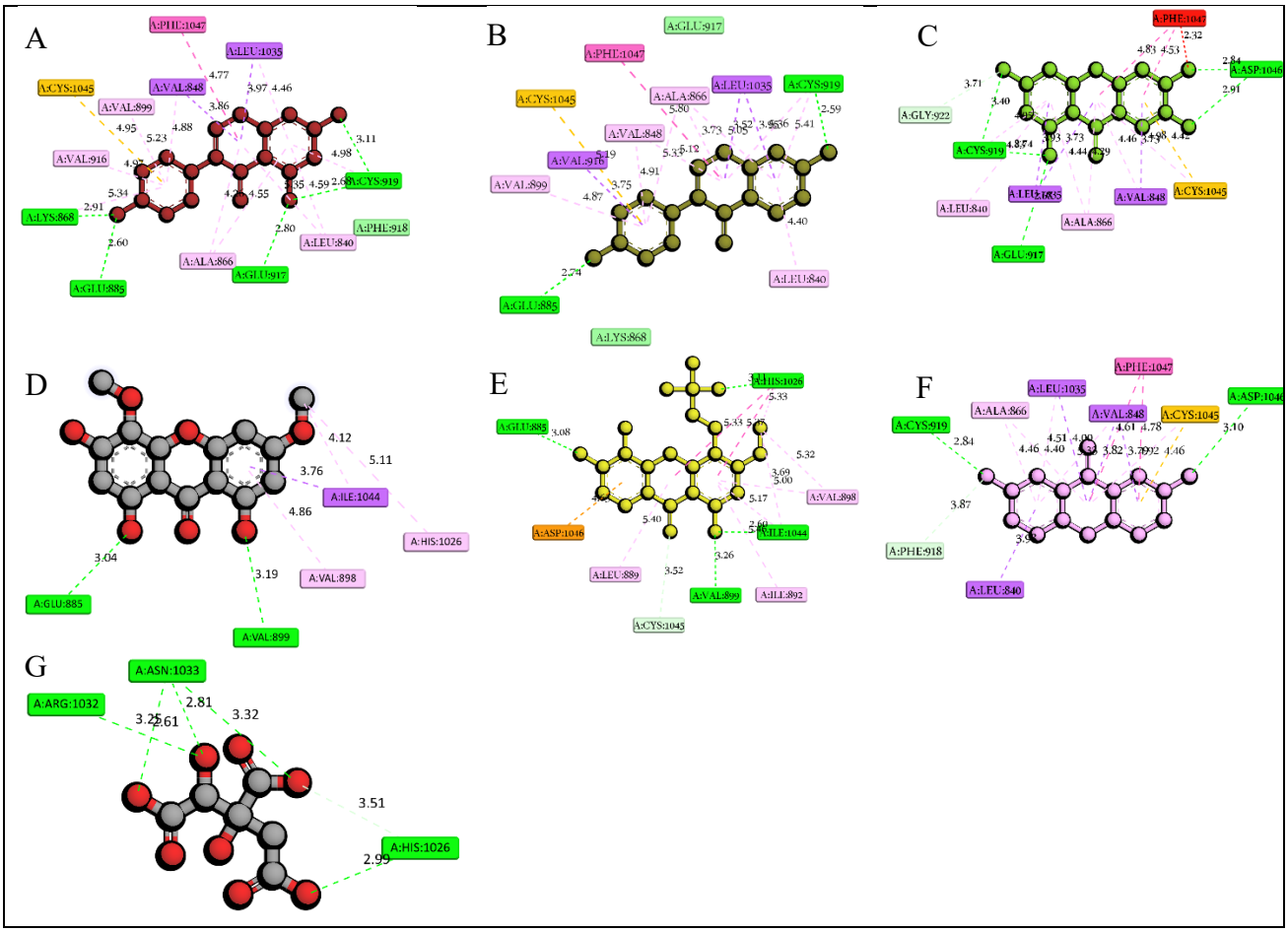

Fig 5: Intramolecular interactions of the top docked compounds within the binding pocket of the receptor (PDB ID: 4AG8). The dashes represent the intramolecular interaction type. The numbers on the dashes represent the distance in Å. A: 5280961, B: 5281708, C: 5281656, D: 71546261, E: 11559542, F: 2836049, G: 13037289.

4. Discussion

VEGFR2 expression across tumor stages showed consistent upregulation across all stages, with the most significant differences observed between Stage 1 and subsequent stages, particularly between Stage 1 and Stage 4. Our analysis revealed that higher VEGFR2 expression does not significantly impact survival outcomes, suggesting variability in its role depending on the cancer type. However, in KIRC, high VEGFR2 expression is associated with significantly improved survival outcomes, with a 39% reduction in disease recurrence risk and a 51% reduction in mortality risk. Several studies have reported VEGFR2 as the target protein for treating cancers, and have marked its high expression in

various cancers [33, 34], therefore, the paradoxical high expression of VEGFR2 associated with OS and DFS in KIRC and other renal system cancers could have arisen due to a lesser number of samples or the early-stage samples studied.

The correlation analysis between VEGFR2 and other genes has provided valuable insights into the genetic landscape associated with this key receptor. The results highlight the extensive network of genetic interactions involving VEGFR2 and its involvement in regulating a wide range of cellular processes critical for endothelial cell function. PPI network analysis revealed its central role in angiogenesis, and in modulating the immune microenvironment. Cross-Talk with Other Signaling Pathways: Associations with CALCRL and RAPGEF4 indicate potential cross-talk between different receptor systems that could be important for understanding the full scope of VEGFR2's biological functions.

The ADMET analysis provides valuable insights into the pharmacokinetic and toxicity profiles of the 11 *G. oblongifolia* compounds. Highly acceptable pharmacokinetic properties obtained for the compound 13037289 suggest that it may improve therapeutic efficacy, but it requires careful dosing to avoid rapid elimination. Compared to Axitinib, Compound 13037289 has good solubility, intestinal absorption, BBB permeability, low PPB, and a high fraction of unbound, which may increase free drug concentrations. Its half-life is shorter and clearance is faster. While Axitinib is protein-bound, has lower intestinal absorption, and a longer half-life, it targets VEGFRs with high potency. These differences suggest that Compound 13037289 may have unique pharmacokinetics. Other compounds with high acceptable ADMET properties are 11559542 and 13037289 that showed no acute aquatic toxicity, indicating no risk to aquatic organisms. Compound 13037289, with a good pharmacokinetic profile, is expected to have a high ADMET score, indicating fewer side effects and better safety than compounds with lower scores. This scoring system helps identify compounds with higher clinical development potential. All compounds except 11559542 and 13037289 showed no acute aquatic toxicity, indicating no risk to aquatic organisms. Genotoxicity assays revealed significant variability among the compounds, with Compound 2836049 showing potential genetic damage and mutagenic effects. Overall, 11559542 is highlighted as a prime candidate for further development as a VEGFR2 inhibitor, with the potential for optimization through medicinal chemistry to improve its potency.

The filtered *G. oblongifolia* compounds were examined for VEGFR2 binding. The well-known VEGFR2 inhibitor axitinib is a Type IVa Tyrosine Kinase Inhibitor (TKI) because it targets the DFG-out conformation and interacts with the kinase channel. Important residues like GLU885, ASP1046, and CYS919 stabilize inhibitors in the ATP-binding site and the Rear Deep Pocket. A comparative interaction analysis of *G. oblongifolia* compounds revealed how they interact with these critical residues [35]. It is well-documented that hydrogen bonds are pivotal for the stabilization of inhibitors

[36]. Axitinib forms key hydrogen bonds with ASP1046 and GLU885, which stabilize the kinase's DFGout conformation and contribute to high selectivity, where the DFG (Asp-Phe-Gly) motif is a key element in the regulation of the kinase activity [2]. Docking revealed that all compounds, including the reference inhibitor Axitinib, fit well into the binding pocket, indicating VEGFR2 binding site compatibility. The docking energies, measured in kJ/mol, indicate the binding affinity of each compound with the VEGFR2 binding pocket. Compounds with lower docking energies exhibited stronger predicted binding affinities, essential for effective inhibitory interactions. Docking studies revealed that similar to Axitinib, these compounds interact with VEGFR2 inhibitor residues ASP1046 and GLU885. For stable binding, 25209069 and 5280961 formed hydrogen bonds with CYS919, ASP1046, and GLU885. The binding strength of axitinib was comparable to the hydrogen bonds formed by 25209069 with CYS919 and GLU917. Axitinib and 5280961 exhibited similar interactions with GLU885 and GLU917, including hydrogen bonding. Axitinib interacted with LEU1035, VAL916, and CYS1045 using pi-sigma, pi-alkyl, and pi-pi. Compounds such as 5281708 and 5281631 exhibited pi interactions with LEU1035 and VAL848, indicating stable hydrophobic pocket positioning. According to the literature, hydrogen bonds between D1046's backbone NH and E885's carboxylate side chain aid in Axitinib binding. 5280961 and 14077269 replicated these interactions, implying that they can inhibit VEGFR2 through a similar binding mode [2]. Specifically, 45269778 and 11559542 maintained pi-pi stacking and alkyl interactions with PHE1047 and CYS1045, which inhibit VEGFR2 and increase binding affinity. Compounds 25209069 (-107.04 kJ/mol) and 45269778 (-106.28 kJ/mol) had slightly higher binding energies than axitinib, which had a binding energy of -99.12 kJ/mol. These compounds may inhibit VEGFR2. Therefore, some of the most promising VEGFR2 inhibitors from *G. oblongifolia* identified are 11559542, 5280961, and 5281656. The structural resemblance to Axitinib in terms of pi interactions and hydrogen bond donors and acceptors points to the inhibition of the VEGFR2 binding pocket.

5. Conclusion

VEGFR2 expression is crucial in various tumor stages, and its increased expression across all stages, with significant demographic variations, suggests it could be utilized as a cancer marker. The study reveals a network of genes associated with VEGFR2, revealing its role in cell proliferation and angiogenesis, and its potential influence on tumor microenvironment and immune evasion mechanisms. The ADMET analysis of *G. oblongifolia* compounds highlights compound 13037289 as a strong candidate due to its favorable pharmacokinetic properties, including good solubility and moderate BBB permeability. In contrast, compounds 11559542 and 14077269 show wider tissue distribution, indicating potential for systemic activity. The docking analysis revealed that several

compounds from *G. oblongifolia* exhibit strong inhibitory effects on VEGFR2, with compounds 25209069 and 45269778 showing lower binding energies than Axitinib, indicating a strong affinity for the VEGFR2 binding pocket. The analysis emphasized the importance of hydrogen bonds and Pi-interactions in stabilizing these inhibitors. Notably, compound 11559542 demonstrated a unique electrostatic Pi-Anion interaction with ASP1046, a critical residue in the kinase's DFG-out conformation, suggesting a potentially novel mechanism for inhibiting VEGFR2. Several compounds from *G. oblongifolia* exhibit moderate inhibitory effects on VEGFR2, showing structural similarities to Axitinib. Compounds 13037289 and 11559542 interactions with key residues GLU885 and ASP1046 suggest that targeted modifications could improve their potency. Additionally, these compounds possess favorable pharmacokinetic and safety profiles, indicating their potential as safer VEGFR2 inhibitors derived from natural sources.

6. Futures Prospects

Various future studies can be applied to achieve the most potent inhibition of VEGFR2 to treat KIRC using natural compounds from *G. oblongifolia*. Optimize VEGFR2 binding affinity and specificity through fragment- and structure-based drug design. These methods can improve compound potency and selectivity by improving key residue interactions. After optimization, in vitro assays can be applied to validate computational predictions, followed by in vivo cancer models to assess pharmacokinetics, tissue distribution, and efficacy. The compounds' real-world efficacy and safety must be confirmed by these steps.

Funding Sources

Not available

Conflict of Interest

The authors share no conflict of interest.

Acknowledgment

The authors are thankful to the Deanship of Graduate Studies and Scientific Research at the University of Bisha for supporting this work through the Fast-Track Research Support Program.

The authors also extend their appreciation to the Deanship of Graduate Studies and Scientific Research at the Islamic University of Madinah for its academic support and contributions.

References

[1] F. Bray et al., "Global cancer statistics 2022: GLOBOCAN estimates of incidence and mortality worldwide for 36 cancers in 185 countries," CA: A Cancer Journal for Clinicians, vol. 74, no. 3, pp. 229-263, 2024.

[2] M. McTigue, B. W. Murray, J. H. Chen, Y. L. Deng, J. Solowiej, and R. S. Kania, "Molecular conformations, interactions, and properties associated with drug efficiency and clinical performance among VEGFR TK inhibitors," Proc Natl Acad Sci U S A, vol. 109, no. 45, pp. 18281-9, Nov 6 2012.
[3] E. Jonasch, C. L. Walker, and W. K. Rathmell, "Clear cell renal cell carcinoma ontogeny and mechanisms of lethality," Nature Reviews Nephrology, vol. 17, no. 4, pp. 245-261, 2021.
[4] (2024, 12 November, 2024). Kidney cancer statistics. Available: https://www.wcrf.org/cancer-trends/kidney-cancer-statistics/
[5] A. Alasker et al., "Exploring Renal Malignancies in Saudi Arabia: Insights from a Tertiary Care Center Study," Journal of Kidney Cancer and VHL, pp. 13-19, 12/21 2023.
[6] N. Ferrara, "VEGF and the quest for tumour angiogenesis factors," Nature Reviews Cancer, vol. 2, no. 10, pp. 795-803, 2002/10/01 2002.
[7] K. Holmes, O. L. Roberts, A. M. Thomas, and M. J. Cross, "Vascular endothelial growth factor receptor-2: structure, function, intracellular signalling and therapeutic inhibition," Cell Signal, vol. 19, no. 10, pp. 2003-12, Oct 2007.
[8] Z.-L. Liu, H.-H. Chen, L.-L. Zheng, L.-P. Sun, and L. Shi, "Angiogenic signaling pathways and anti-angiogenic therapy for cancer," Signal Transduction and Targeted Therapy, vol. 8, no. 1, p. 198, 2023/05/11 2023.
[9] L. Perez-Gutierrez and N. Ferrara, "Biology and therapeutic targeting of vascular endothelial growth factor A," Nat Rev Mol Cell Biol, vol. 24, no. 11, pp. 816-834, Nov 2023.
[10] P. Carmeliet and R. K. Jain, "Molecular mechanisms and clinical applications of angiogenesis," Nature, vol. 473, no. 7347, pp. 298-307, May 19 2011.
[11] K. R. Molhoek et al., "VEGFR-2 expression in human melanoma: revised assessment," Int J Cancer, vol. 129, no. 12, pp. 2807-15, Dec 15 2011.
[12] D. Sia, C. Alsinet, P. Newell, and A. Villanueva, "VEGF signaling in cancer treatment," Curr Pharm Des, vol. 20, no. 17, pp. 2834-42, 2014.
[13] M. Gross-Goupil, L. Francois, A. Quivy, and A. Ravaud, "Axitinib: a review of its safety and efficacy in the treatment of adults with advanced renal cell carcinoma," Clin Med Insights Oncol, vol. 7, pp. 269-77, Oct 29 2013.
[14] S. Shyam Sunder, U. C. Sharma, and S. Pokharel, "Adverse effects of tyrosine kinase inhibitors in cancer therapy: pathophysiology, mechanisms and clinical management," Signal Transduct Target Ther, vol. 8, no. 1, p. 262, Jul 7 2023.
[15] W. G. Shan, T. S. Lin, H. N. Yu, Y. Chen, and Z. J. Zhan, "Polyprenylated Xanthones and Benzophenones from the Bark of Garcinia oblongifolia," Helvetica Chimica Acta, vol. 95, 08/01 2012.
[16] K. S. Triyasa, A. Diantini, and M. I. Barliana, "A Review of Herbal Medicine-Based Phytochemical of Garcinia as Molecular Therapy for Breast Cancer," Drug Des Devel Ther, vol. 16, pp. 3573-3588, 2022.
[17] R. P. Hertzberg, M. J. Caranfa, and S. M. Hecht, "On the mechanism of topoisomerase I inhibition by camptothecin: evidence for binding to an enzyme-DNA complex," Biochemistry, vol. 28, no. 11, pp. 4629-4638, 1989.
[18] H. O. Fearnhead, M. Chwalinski, R. T. Snowden, M. G. Ormerod, and G. M. Cohen, "Dexamethasone and etoposide induce apoptosis in rat thymocytes from different phases of the cell cycle," Biochemical pharmacology, vol. 48, no. 6, pp. 1073-1079, 1994.
[19] P. Li et al., "Comparative UPLC-QTOF-MS-based metabolomics and bioactivities analyses of Garcinia oblongifolia," Journal of Chromatography B, vol. 1011, pp. 179-195, 2016.
[20] D. Brawand et al., "The evolution of gene expression levels in mammalian organs," Nature, vol. 478, no. 7369, pp. 343-348, 2011/10/01 2011.
[21] Z. Tang, B. Kang, C. Li, T. Chen, and Z. Zhang, "GEPIA2: an enhanced web server for large-scale expression profiling and interactive analysis," Nucleic acids research, vol. 47, no. W1, pp. W556-W560, 2019.
[22] K. Tomczak, P. Czerwińska, and M. Wiznerowicz, "Review The Cancer Genome Atlas (TCGA): an immeasurable source of knowledge," Contemporary Oncology/Współczesna Onkologia, vol. 2015, no. 1, pp. 68-77, 2015.
[23] J. Lonsdale et al., "The genotype-tissue expression (GTEx) project," Nature genetics, vol. 45, no. 6, pp. 580-585, 2013.
[24] D. S. Chandrashekar et al., "UALCAN: a portal for facilitating tumor subgroup gene expression and survival analyses," Neoplasia, vol. 19, no. 8, pp. 649-658, 2017.
[25] J. Koster, R. Volckmann, D. Zwijnenburg, P. Molenaar, and R. Versteeg, "R2: Genomics analysis and visualization platform," Cancer Research, vol. 79, no. 13_Supplement, pp. 2490-2490, 2019.
[26] D. Szklarczyk et al., "The STRING database in 2021: customizable protein–protein networks, and functional characterization of user-uploaded gene/measurement sets," Nucleic acids research, vol. 49, no. D1, pp. D605-D612, 2021.
[27] X. Yin et al., "CODD-Pred: A Web Server for Efficient Target Identification and Bioactivity Prediction of Small Molecules," Journal of Chemical Information and Modeling, vol. 63, no. 20, pp. 6169-6176, 2023.
[28] K.-C. Hsu, Y.-F. Chen, S.-R. Lin, and J.-M. Yang, "iGEMDOCK: a graphical environment of enhancing GEMDOCK using pharmacological interactions and post-screening analysis," BMC Bioinformatics, vol. 12, no. 1, p. S33, 2011/02/15 2011.

[29] M. Shibuya, "Vascular Endothelial Growth Factor (VEGF) and Its Receptor (VEGFR) Signaling in Angiogenesis: A Crucial Target for Anti- and Pro-Angiogenic Therapies," Genes Cancer, vol. 2, no. 12, pp. 1097-105, Dec 2011.
[30] C. S. Abhinand, R. Raju, S. J. Soumya, P. S. Arya, and P. R. Sudhakaran, "VEGF-A/VEGFR2 signaling network in endothelial cells relevant to angiogenesis," J Cell Commun Signal, vol. 10, no. 4, pp. 347-354, Dec 2016.
[31] S. Kdimati, C. S. Mullins, and M. Linnebacher, "Cancer-Cell-Derived IgG and Its Potential Role in Tumor Development," Int J Mol Sci, vol. 22, no. 21, Oct 27 2021.
[32] J. Ma et al., "Signaling pathways in vascular function and hypertension: molecular mechanisms and therapeutic interventions," Signal Transduction and Targeted Therapy, vol. 8, no. 1, p. 168, 2023/04/20 2023.
[33] Y. Yang and Y. Cao, "The impact of VEGF on cancer metastasis and systemic disease," Seminars in Cancer Biology, vol. 86, pp. 251-261, 2022/11/01/ 2022.
[34] T. R. Holzer et al., "Tumor cell expression of vascular endothelial growth factor receptor 2 is an adverse prognostic factor in patients with squamous cell carcinoma of the lung," PLoS One, vol. 8, no. 11, p. e80292, 2013.
[35] R. S. Kania, "Structure-Based Design and Characterization of Axitinib," Kinase inhibitor drugs, pp. 167-201, 2009.
[36] M. Majewski, S. Ruiz-Carmona, and X. Barril, "An investigation of structural stability in protein-ligand complexes reveals the balance between order and disorder," Communications Chemistry, vol. 2, no. 1, p. 110, 2019/09/17 2019.